New Approach to Predicting Local Scour Downstream of Grade-Control Structure

New approach predicting local scour downstream of a grade-control structure

M. Ben Meftah[1*], M. Mossa[2]

[1]Assistant Professor, Department of Civil, Environmental, Land, Building Engineering and Chemistry, Polytechnic University of Bari, Via E. Orabona 4, 70125 Bari, Italy ([*]Corresponding author). E-mail: mouldi.benmeftah@poliba.it,

[2]Full Professor, Department of Civil, Environmental, Land, Building Engineering and Chemistry, Polytechnic University of Bari, Via E. Orabona 4, 70125 Bari, Italy. E-mail: michele.mossa@poliba.it

Abstract

Despite the numerous studies on scouring processes, prediction of scour hole dimensions downstream of hydraulic structures always remains challenging because of the complexity of the phenomenon and its dynamic sensitivity to structure and sediment properties.

In this study, we experimentally focus on the scour hole development downstream of a sloped grade-control structure (GCS) in alluvial channels. A large series of laboratory experiments were carried out in a rectangular channel with a non-cohesive sediment bed. Based on the data of the present study and in addition to data collected from previous studies, the effect of the downstream-face slope of the GCS on the scour morphology was analyzed. In this regard, it was found that the face-slope takes effect only if it is smaller than the slope of the upstream equilibrium-scour side obtained with a GCS of vertical downstream-face. Before reaching an equilibrium state, the scour process evolves into three distinct phases, including a very rapid initial phase, an intermediate gradual phase, and an equilibrium phase. A general empirical expression for predicting the temporal scour evolution is proposed and extended to different types of GCS.

Moreover, we propose a new scaling approach that leads to the derivation of new equations predicting the equilibrium-scour profiles with different entering jet-flow typologies. To make these

equations operational, we also propose a series of estimating expressions for the characteristic lengths of the equilibrium-scour hole.

Keywords: Grade-control structure, non-cohesive sediments, entering jet-flow, local scour, temporal evolution, new scaling approach, equilibrium profile, scour lengths.

Introduction

Grade-control structures (GCSs) are considered to be one of the most important ways to prevent excessive degradation and erosion in alluvial channels (Bormann and Julien, 1991). A typical GCS is 1.5 - 2 m higher than the original riverbed (Lu et al., 2013), often leading to a critical flow condition over the GCS followed by a downstream supercritical condition, forming a jet that enters the channel. The potential erosive action of this jet causes considerable downstream local scour, which may give rise to an instability of the structure. A full understanding of the scouring process and predicting the scour evolution is a critical design consideration.

Local scour downstream of hydraulic GCSs, i.e., bridge piers and abutments, sills, sluice gates, spillways, weirs, etc. has drawn attention and interest from many researchers (e.g., Schoklitsch, 1932, Veronese, 1937; Laursen, 1952; Carstens, 1966; Martins, 1975; Mason and Arumugam, 1985; Bormann and Julien, 1991; Mossa, 1998; Hopfinger et al., 2004; Ben Meftah and Mossa, 2006; Hill and Younkin, 2006; Tregnaghi et al., 2007; Guven and Gunal, 2008; Pagliara et al., 2011; Scurlock et al., 2012; Pagliara and Palermo, 2013; Guan et al., 2014; Guan et al., 2016; Shafai-Bejestan et al., 2016; Fakhari and Kabiri-Samani, 2017). Most of these studies have focused on the prediction of scour features at the equilibrium stage, such as the maximum depth and length of the scour, because of their importance in designing hydraulic structures. Other studies (Kuhnle et al., 2002; Nasrollahi et al., 2008; Chen et al., 2016; Papanicolaou et al., 2018) are dedicated to the evolving process of the scour hole as a function of time. The flow field in the scour-pool is very

complex, involving the development of three-dimensional vortex structures, which affect and are affected by the scour morphology.

Since the scour hole is a consequence of the interaction between the flow-hydrodynamic structures and the GCS, predicting the equilibrium-scour hole dimensions should be based on the characteristic flow parameters (upstream and downstream of the scour hole) and the GCS-features. The early study of Schoklitsch (1932) proposed some empirical formulae to predict the maximum eroded depth, considering the unit discharge and the height difference between head and tailwater level as parameters related to the impact forces on the bed and the non-cohesive sediment size as a resistance parameter. Later studies (e.g., Mason and Arumugam, 1985; Bormann and Julien, 1991) focused on the effects of the entering jet-flow on the maximum scour dimensions. Tregnaghi et al. (2007) argued that the scour process is time-dependent and usually reaching its equilibrium stage rapidly in live-bed conditions and rather slowly in clear-water conditions. Lu et al. (2013) argued that, based on experimental results of steady and unsteady flows, the scour evolving process downstream of a GCS is divided into three distinct phases, including an initial phase, a developing phase, and an equilibrium phase. Confirming observations were reported by Ben Meftah and Mossa (2006) and Tregnaghi et al. (2007). Lu et al. (2013) indicated that, in steady flow, the scour hole in non-cohesive sediments is primarily influenced by the channel bed slope, the densimetric Froude number, the tailwater depth, and the sediment median size.

Most studies on scouring process downstream of hydraulic structures (e.g., Bormann and Julien, 1991; Gaudio et al., 2000; Ben Meftah and Mossa, 2006; Tregnaghi et al., 2007; Lu et al., 2013) asserted that the scour hole profiles are similar in shape, giving rise to a typical profile with appropriate scaling of the horizontal and vertical coordinates.

The flow field measurements showed the development of secondary currents at the cross-section of maximum scour depth (Ben Meftah and Mossa, 2006; Guan et al., 2014). These secondary flows have a considerable effect on the final geometry of the scour hole and create the

greatest scour depth close to the side wall rather than at the flume centerline. The mechanism of secondary currents (origin, strength, direction of motion and interaction with sediment bed) in open channel flows has been deeply discussed by Yang et al. (2012), indicating the dependence of the secondary currents on the channel geometry, such as the aspect ratio and roughness distributions.

Since the prediction of the scour features remains challenging due to the complexity of the phenomenon, in the present study, we will experimentally focus on the scour hole development downstream of a GCS in sand-bed channels. The main objectives of these experiments, and with the help of referencing data collected from previous studies, are to present more general formulas to easily predict the scour temporal evolution and the equilibrium-scour profile .

Dimensional analysis and review of scour prediction approaches

For clear-water, the equilibrium phase of the scour process is defined as the condition when the scour dimensions do not vary with time. Due to flow turbulence, variations within equilibrium-scour depth may occur. According to Mason and Arumugan (1985), these variations are relatively small, and the concept of a maximum scour depth is acceptable and adaptable for engineering design consideration. Previous laboratory experiments have indicated that the scour hole may take several hours or days to attain its equilibrium condition. Fig. 1 is a schematic sketch of the equilibrium-scour hole downstream of a GCS, in which a free entering jet-flow of initial thickness h_s and mean velocity U_0 (at the tailwater entering) plunges into the scour pool along with a path L_s, defined as the diffused length of the jet. Herein, h_t indicates the tailwater depth above the unscoured bed level, q is the unit water discharge, (x, z) are the longitudinal and vertical coordinates, respectively, x_s is the horizontal distance from the face of the GCS to point of maximum equilibrium-scour depth, z_s is the maximum scour depth at equilibrium, z_d is the drop height of the GCS, α is the maximum side angle of the scour hole, β is the jet angle near the bed, λ is the

downstream face angle of the GCS. It is worth mentioning that the (x, z)-coordinates originate at the original bed level from the beginning of the GCS face along the channel axis (as shown in Fig. 1).

Due to the large velocity gradients between the jet-flow and that in the scour pool, near the bed the jet diffuses and is redirected at a reduced bed velocity. When the drag force generated by this velocity exceeds the submerged sediment particle weight force, motion and transport of sediments occur. The equilibrium state happens when the path of the impinging jet becomes sufficiently long and its diffused velocity is reduced to a value smaller than the minimum value required for transport (Scurlock et al., 2012). Pagliara and Palermo (2013) observed that the flow regime (occurrence of hydraulic jump in scour pool) deeply influences the scour process. With sediments of density ρ_s and standard size d_{50} (grain size for which 50% of the total weight of the sediment is finer), the effective parameters on the scour phenomenon downstream of a GCS in alluvial channels can be represented by the following relationship:

$$l_s, x_s, z_s = f(d_{50}, h_s, h_t, g, q, z_d, \lambda, \nu, \rho_s, \rho_w) \quad (1)$$

where g is the gravitational acceleration, l_s is the equilibrium-scour length, ν is the kinematic water viscosity and ρ_w is the water density.

The application of dimensional analysis to the variables of Eq. (1) leads to the following dimensionless expression:

$$\frac{l_s}{h_s}, \frac{x_s}{h_s}, \frac{z_s}{h_s} = f\left(\frac{d_{50}}{h_s}, \frac{h_t}{h_s}, \frac{z_d}{h_s}, \frac{1}{Fr_s^{\,2}}, \frac{1}{Re}, \lambda, \frac{\rho_s - \rho_w}{\rho_w}\right) \quad (2)$$

where $Fr_s = q/[h_s(gh_s)^{0.5}]$ is the Froude number at the crest-end of flow depth h_s (Fig. 1). For fully turbulent flow, the dependence upon the Reynolds number, $Re = q/\nu$, could be neglected, and thus Eq. (2) can be finally expressed as follows:

$$\frac{l_s}{h_s}, \frac{x_s}{h_s}, \frac{z_s}{h_s} = f\left(\frac{h_t}{h_s}, \frac{z_d}{h_s}, \lambda, \frac{q}{h_s\sqrt{(\Delta-1)gd_{50}}} = Fr_{sd}\right) \quad (3)$$

where Fr_{sd} is the densimetric Froude number and $\Delta = \rho_s/\rho_w$. Note that Fr_{sd} is obtained combining the three parameters d_{50}/hs, Fr_s and $(\rho_s-\rho_w)/\rho_w$.

Despite the several studies on local scour erosion downstream of hydraulic structures, prediction of the equilibrium-scour features is always very uncertain. Most of the earliest scour-depth equations, applicable for GCS, are summarized in Mason and Arumugam (1985). Based on the measurement of physical models and prototypes, Mason and Arumugam (1985) proposed a more precise formula to predict the maximum scour depth as:

$$z_s + h_t = K \frac{q^a H^b h_t^c}{g^e d_{50}{}^f} \tag{4}$$

where H is the head drop, a difference between the headwater depth upstream the GCS and the tailwater level (Fig. 1). For a complete model and prototype expression, the appropriate values of K and the exponents a, b, c, e and f, in Eq. (4), can be evaluated as: $K = 6.42 - 3.10H^{0.10}$; $a = 0.60 - H/300$; $b = 0.15 - H/200$, $c = 0.15$, $e = 0.30$; and $f = 0.10$ (with an assumed constant value for $d_{50} =$ 0.250 m for prototypes).

Bormann and Julien (1991) proposed a semi-theoretical expression, based on a large-scale experimental study and a theoretical analysis of the local scour caused by a typically two-dimensional jet flow diffusion, generated by the GCS, and the particle stability in the scour hole as:

$$z_s + z_d = Kq^{0.6} \frac{U_o}{g^{0.8} d_{50}{}^{0.4}} \sin(\beta) \quad \propto \quad K \frac{q^{1.6}}{H_c g^{0.8} d_{50}{}^{0.4}} \sin(\beta) \tag{5}$$

where $K = C_d^2[\sin\phi/(\sin(\phi + \alpha)B'(\Delta - 1)g]^{0.8}$, B' is a coefficient of friction relationship, ϕ is the submerged angle of repose of bed sediment and C_d is the jet diffusion coefficient (with values ranging from 2.0 to 2.4).

Using a wide range of experimental data and based on dimensional analysis, D'Agostino and Ferro (2004) proposed an empirical expression of the maximum scour depth as follows:

142 $$\frac{z_s}{z_d} = 0.54\left(\frac{b_s}{z_d}\right)^{0.593}\left(\frac{h_t}{H}\right)^{-0.126}(A_{50})^{0.544}\left(\frac{d_{90}}{d_{50}}\right)^{-0.856}\left(\frac{b_s}{B}\right)^{-0.751} \quad (6)$$

143 Where $A_{50} = Q/b_s z_d[gd_{50}(\Delta - 1)]^{1/2}$, Q is the water discharge, B is the width of the mean channel,
144 which may differ from the width of the GCS b_s, and d_{90} is the bed grain size for which 90% of
145 sampled particles are finer.

146

147 **Experimental set-up**

148 The experiments on the scour processes were carried out in a rectangular flume at the
149 Hydraulic Laboratory of the Mediterranean Agronomic Institute of Bari (Italy). The flume has glass
150 sidewalls and a Plexiglass floor. It is 7.72 m long, 0.30 m wide, and 0.40 m deep. A pump of
151 maximum discharge of 25 *l*/s was used to deliver water from the laboratory sump to an upstream
152 tank equipped with a baffle and lateral weir, maintaining a constant head upstream of a movable
153 slide-gate constructed at the inlet of the flume. The slide-gate regulates channel flow-discharge. At
154 the outlet of the flume, water is intercepted by a stilling tank, equipped with three vertical grids to
155 stabilize water, and a triangular weir (V-notch sharp crested weir) to measure discharge with
156 relative uncertainty of ±8%.

157 The GCS consists of a wooden model structure of a longitudinal trapezoidal-shape and has the
158 same width of the flume. The upstream face of the GCS is sloped 1H:1V, in order to create a
159 smooth flow transition over the GCS. The GCS is 0.25 m high with a crest length of 0.85 m and a
160 width equal to that of the channel. Three downstream faces of the GCS were tested in the present
161 study; a vertical face, a 1H:1V slope and a 3H:1V slope (see Fig. 2).

162 The flume bottom downstream of the GCS model is covered with a 0.16 m thick, 4 m long
163 layer of erodible bed material consisting of almost uniform sand particles with mean average size
164 (d_{50}) of 2 mm and density of 2650 kg/m^3. The erodible bed terminates with a piece of wood of
165 height equal to the thickness of the sand layer, downstream tapered to the channel bottom to

166 minimize flow disturbance. At the downstream end of the flume, a movable gate, made of Plexiglas
167 and hinged at the channel bottom, is used to regulate the flow depth (Fig. 2)

168 The data collected during each test included discharge, water surface elevation, flow depth,
169 temporally eroded bed profile, equilibrium-bed profile and scour dimensions (depth, length, the
170 position of maximum depth). The profiles of the equilibrium-eroded bed along the channel
171 centerline, near the channel sidewalls, and at intermediate distance between the channel centerline
172 and both sidewalls (Fig. 2) was measured, as the vertical distance between the initial bed elevation
173 and the bed at equilibrium stage, by means of a point gage of ±0.1 mm accuracy. Whereas, the
174 water level profile along the channel centerline was measured using an electrical hydrometer with
175 an accuracy of ±0 .1 mm.

176 The main experimental parameters of the present study are illustrated in Table 1. The maximum
177 scour depth was determined as the vertical distance between the initial bed profile and the lowest
178 position of the equilibrium-scour hole at the centerline (channel axis). The scour length was
179 determined as the longitudinal distance from the downstream face of the GCS to the position at
180 which the equilibrium-scour reaches the initial bed profile (Fig. 1).

181

182 **Results and discussion**

183 *Temporal evolution of the scour hole*

184 Due to the high velocity of the jet from the GCS, a scour hole begins to form downstream of
185 the GCS. At the beginning (first few minutes) of all the experiments, it was observed that the scour
186 hole rapidly expands with time. With the passing of time, the scouring rate (profile variation with
187 time) gradually decreases until reaching an equilibrium condition. In the present study, the data of
188 the scour profiles at different time intervals were collected, by tracing them on the right channel-
189 wall. Figs. 3a)-3c) report, as an example, the variation of the scour profiles with time advance in the
190 case of the GCS with vertical (λ = 90°), 1H:1V (λ = 45°) and 3H:1V (λ = 18°) downstream face

slopes, respectively. In Fig. 3 the data correspond to runs R3, R19 and R26. From the values of q and h_t in Table 1, it can be noted that the temporal scour profiles with the different slopping faces, illustrated in Fig 3, were obtained with nearly the same hydraulic conditions. This allows us to easily identify any possible λ-effect on the scour features. Fig. 3 shows the quasi-complete erosion of the sediment materials from the GCS-face with 1H:1V and 3H:1V slopes. The λ-effect is more pronounced with the 3H:1V slope of smallest λ-value. This is clearly shown at t = 60 mn, as an example, where the largest scour depth takes place on the face of the GCS with λ = 18° (Fig. 3c), whereas with λ = 45° it occurs a few centimeters downstream of the GCS-face (Fig. 3b).

In order to better show the λ-effect on the scour features, in Fig. 4 we plot the scour profiles obtained after the same time-intervals for the three face-slopes. The data refer to t = 60 mn and t = 120 mn for runs R3, R19 and R26. Note that in Fig. 4, the scour depth is plotted as a function of $X = x\text{-}x'$, where x' is defined as the base length of the downstream GCS-face (triangular shaped) at the original-bed level (see Fig. 1). Fig. 4 clearly shows a considerable change in the scour-dimensions by varying the impact angle (λ). As λ decreases, the scour hole, after the same time-interval, extends further downstream of the GCS. At t = 60 mn, as an example, the scour length, at z = 0, is increased by almost 8% and 32% with λ = 45° and 18°, respectively, by referring to the scour obtained with the vertical face. This indicates that, at small λ-values, the scour hole grows more rapidly in the downstream direction. It should be noted that, after 120 mn, the scour hole with the vertical and 1H:1V sloped face (runs R3 and R19) reaches more than 95% of its equilibrium depth against almost 75% with the 3H:1V sloped face (run R26). For this reason, in Fig. 4 we also plot the equilibrium-scour profile (t = 840 mn) of the 3H:1V sloped face. Finally, a slight increase in the equilibrium maximum eroded-depth is observed with the decrease of λ. This finding is in agreement with Pagliara et al. (2008a, 2008b) on the effect of inclined jet flow on scouring features, arguing that the effect of the jet impact angle is almost inversely quadratic, i.e., smaller angles produce a deeper and longer scour hole as do larger jet impact angles. Recently, Wang et al. (2018), studied

local scour at downstream sloped submerged weirs in a sand-bed channel, observed that the downstream face-slope of the GCS has an effect on the scour hole dimensions only if it is smaller than the slope of the upstream side of the scour hole obtained with the vertical weirs. The authors indicated that, when λ is larger than the upstream scour side angle caused by the vertical face, the overflow properties are almost similar to those obtained with the vertical weir and the downstream sloped-face surface is fully covered by sediments.

Fig. 5 illustrates the nondimensional equilibrium-scour profiles at different transversal positions. The scour depth z is normalized by the absolute value of the maximum equilibrium-scour depth at the channel-centerline $|z_s|$, while the downstream position X is normalized by the maximum scour length l_s. The profiles correspond to runs R2, R14 and R24, with λ = 90°, 45° and 18°, respectively. The scour profiles were measured, starting from the channel right wall, at the transversal positions of y = -13, -6, 0, 6 and 13 cm, as respectively denoted by R, CR, C, CL and L in Fig. 2. Fig. 5 shows an almost transversal symmetry of the eroded bed with respect to the flume axis (centerline C). Similar results were also obtained in previous studies by Adduce and Sciortino (2006), Ben Meftah and Mossa (2006), Farhoudi and Shayan (2014). From the examination of Fig. 5, and according to the results obtained herein, the maximum-scour hole appears slightly deeper, by almost 12% with λ = 90° and 10% with both λ = 45° and 18°, near the flume sidewalls than at the centerline position. Farhoudi and Shayan (2014) argued that this is likely due to random flow velocities over the GCS, however, Ben Meftah and Mossa (2006) and Guan et al. (2014), measured flow velocity at different cross sections, asserted that the slight increase of the scour depth near the sidewalls is due to the development of secondary flows, characterized by quasi-symmetrical paired circular flow cells, located at both sides of the centerline sand ridge at the position of maximum scour depth. Yang et al. (2012) indicated that secondary currents play a dominant role in sand ridges and stripes' formation in bed rivers. They concluded that the near-bed secondary flow is always from lower (near boundary regions) to higher (main flow at the channel centerline) velocity zone,

241 which may explain the slight increase of the scour hole near the sidewalls. Yang et al. (2012)
242 justified that the ridges' formation may increase the strength of secondary flow.

243 Fig. 6 shows the time evolution of the scour depth for the present study compared to previous
244 results obtained by Ben Meftah and Mossa (2006) and Chen et al. (2016). The temporal maximum
245 scour depth z_m is normalized by z_s and its corresponding time t is normalized by the time required to
246 achieve the equilibrium state t_e. The experimental data of Ben Meftah and Mossa (2006) were taken
247 for scour holes downstream of rectangular-vertical bed sills in low-gradient channels, whereas those
248 of Chen et al. (2016) were collected downstream of a drop structure with a sloped face. All the data
249 illustrated in Fig. 6 were obtained along the channel axis ($y = 0$).

250 Fig. 6 indicates that the scour hole evolves following three distinct phases: i) a very rapid initial
251 phase, where the scour depth roughly attains 70 % of z_s, for a time less than 10% of t_e; ii) an
252 intermediate phase until the time at which the scour depth almost reaches 90% of z_s. Throughout
253 this phase, the scouring process evolves gradually for a time of almost 40% of t_e; and iii) an
254 equilibrium phase, during which the scour hole only evolves by 10% to reach equilibrium over a
255 time of almost 50% of t_e.

256 The analysis of Fig. 6 shows that the data of the initial and equilibrium phases of the temporal
257 scour evolution, for the different studies, follow a similar trend, independent of the structure
258 features and the initial hydraulic conditions. The data of the intermediate phase, however, show
259 considerable scattering. This scattering seems to be influenced by the grade structure features. The
260 scour hole, in the intermediate phase, generally evolves more slowly with the bed sills in Ben
261 Meftah and Mossa (2006), where, for example, the scour depth increases by almost 7% in Ben
262 Meftah and Mossa (2006) against 10% in the present study for t/t_e ranging between 0.16 and 0.26. It
263 is worth noting that in Ben Meftah and Mossa (2006) the drop height z_d (Fig. 1) is equal to zero and
264 the bed sediment consisted of very coarse sand particles of mean average size d_{50} = 1.8 mm and
265 density of 2650 kg/m^3, (similar to the sediment-characteristics used in this study). In the present

266 study and that of Chen et al. (2016), the important value of z_d increases the flow impact on the
267 mobile bed. A greater impact force can induce a deeper scour hole (Chen et al., 2016). It is worth
268 mentioning that in Chen et al. (2016) the sediment used consisted of medium sand particles of mean
269 average size d_{50} = 0.5 mm

270 Numerous empirical equations have been proposed in the literature to estimate the evolution of
271 the scour hole with time (Kuhnle et al., 2002; Chen et al., 2016). According to Nasrollahi et al.
272 (2008), a general expression of the temporal scour evolution is reproduced as follows:

273 $$\frac{z_m}{z_s} = 1 - \exp\left[-a\left(\frac{t}{t_e}\right)^b\right] \quad (7)$$

274 where a and b are constants to be found experimentally. The bold solid line in Fig. 6 is the solution
275 of Eq. (7) with a = 3.6 and b = 0.45, representing the scour hole evolution with time for the
276 different study cases with an error ranging from less than 1% to 60%. The maximum errors appear
277 in the intermediate phase and decrease as t/t_e increases. The dashed lines in Fig. 6 indicate the lower
278 and upper maximum deviation from the best fit line of Eq. (7), obtained with a = 3.6 and b = 0.45,
279 varying the coefficients a by ±22% and b by ±34% (upper deviation increasing a and decreasing b,
280 lower deviation decreasing a and increasing b). The uncertainty in estimating the temporal scour
281 evolution by Eq. (7) can be reduced by treating separately the data for each study case. With a = 3
282 and b = 0.35, Eq. (7) estimates more accurately (with an error ranging from less than 1% to 15%)
283 the scour hole evolution obtained by Chen et al. (2016). The scour hole evolution downstream of
284 bed sills, reported in Ben Meftah and Mossa (2006), can be predicted better with a = 3.5 and b =
285 0.5, with an error ranging from less than 1% to 45%. According to the results of the present study
286 and those conducted previously by Ben Meftah and Mossa (2006), Chen et al. (2016), Eq. (7) is
287 valid for GCS of vertical or inclined downstream face in sand (medium to very coarse)-bed rivers.
288 Similar trend of the time scour-evolution was also observed by Papanicolaou et al. (2018) around
289 sloped-crest structures, known as barbs, in gravel bed rivers. This implies that Eq. (7) can be

adapted to gravel bed rivers and to different GCS geometries, defining only the suitable values of the coefficients a and b in Eq. (7).

In order to gain a better understanding of possible λ-effects on the time evolution of the scour hole, in Fig. 7 we only plot the data of the present study. Fig. 7 indicates that, with $\lambda = 90°$ and 45°, the data of both configurations follow a similar trend, predictable by Eq. (7) with $a = 3.7$ and $b = 0.35$ (bold solid line in Fig. 7) and of an error ranging from less than 1% to 25%. By increasing/decreasing a by 12% from 3.7 and decreasing/increasing b by 30% from 0.35 we obtain the upper/lower maximum deviation, respectively, from the best fit line (bold solid line), as indicated in Fig. 7 by the dashed lines. At $\lambda = 18°$, in the intermediate phase, a quite downward deviation of the data from the predicted curve (bold solid line) is clearly noted, especially with run R26. This indicates that the decrease of λ below a certain level, smaller than the slope of the upstream side of the scour hole obtained with the vertical face (Wang et al., 2018), has a considerable influence on the scour hole evolution.

Similarity of the scour profile

A possible prediction of the scour-hole shape has important implications on the estimation of the eroded volume (Tregnaghi et al., 2007) for practitioners. By the scaling of the horizontal and vertical scour coordinates, several previous studies (e.g., Balachandar and Kells, 1997; Gaudio et al., 2000; Adduce and Sciortino, 2006; Ben Meftah and Mossa, 2006; Tregnaghi et al., 2007; Farhoudi and Shayan, 2014; Espa and Sibilia 2014) demonstrated that the profiles of the equilibrium-scour holes are similar, i.e., the different profiles collapse onto each other, forming an almost characteristic profile. Most of these studies scaled the vertical coordinate z of the eroded depth by z_s and the horizontal distance X from the source (GCS-face) by x_s or by l_s. The use of such a scaling mode in reality does note force different scour profiles to collapse into a single characteristic profile. The scaling of X by x_s only forces the profiles of the upstream scour-side ($X \leq$

315 x_s) to begin and end on similar values, while a certain scatter between profiles, even if it is not
316 always distinct, should happen along the downstream scour-side ($X \geq x_s$), as shown as an example in
317 Balachandar and Kells (1997). On the other hand, scaling X by l_s does not allow the scour profiles
318 to occur at the same value of the normalized maximum scour depth ($X = x_s)/l_s$.

319 In order to avoid this problem of incomplete-similarity between the scour-hole profiles, in the
320 present study, a new scaling approach is proposed, scaling the equilibrium profile as z/z_s vs. X/x_s for
321 the upstream scour-side, and z/z_s vs. $[1 + (X - x_s)/(l_s - x_s)]$ for the downstream scour-side. This new
322 scaling approach is useful to improve the similarity of the scour profiles, helping us to find a closed-
323 form expression predicting the equilibrium-scour profile.

324 Fig. 8 reports the scour-hole profiles at equilibrium, normalized following the new scaling
325 approach above mentioned, for the present study and previous studies by Balachandar and Kells
326 (1997), Adduce and Sciortino (2006), Ben Meftah and Mossa (2006), Ghodsian et al. (2012) and
327 Espa and Sibilia (2014). It is worth mentioning that the scour hole in Balachandar and Kells (1997)
328 is caused by a turbulent Horizontal (plane) jet-flow downstream of a submerged sluice gate in sand-
329 bed channel of d_{50} ranging between 0.84 and 1.12 mm. The scour-hole profiles by Adduce and
330 Sciortino (2006) were obtained downstream of a GCS followed by a rigid apron in clear water
331 conditions and sand bed of d_{50} = 0.72 mm. The long rigid apron positioned upstream of the erodible
332 bed produces a sort of two-dimensional horizontal inflow jet. The data of Espa and Sibilia (2014)
333 were obtained under almost similar experimental configurations of Adduce and Sciortino (2006)
334 with bed of sand sediments of d_{50} = 0.72 mm. The scour profiles by Ghodsian et al. (2012),
335 however, were the results of free-fall jets generated by a GCS of a vertical downstream face, but of
336 a width smaller than the channel width, in sand-bed channel of d_{50} = 1.28 mm. Despite the
337 difference in conditions under which the scour hole was developed for each case, Fig. 8 indicates
338 that all the scour-profiles of the present and previous studies are fundamentally restricted between
339 three well-defined coordinates (0,0), (1,-1) and (2,0), confirming the good similarity of the scour

340 profile by scaling it in this way. The data scattering in Fig. 8 is related to the scour-shape, which is
341 affected in part by the GCS geometry as well as by the entering jet-flow properties.

342 The examination of Fig. 8 shows that the upstream and downstream sides of the scour profile
343 are slightly asymmetric. At the upstream side, most of the data of the different studies seem to
344 collapse into a single profile, except those of Ghodsian et al. (2012), which are deflected upwards.
345 This data set shows an almost linear trend similar to the case of a GCS of downstream face
346 completely exposed to the flow, as shown by the dotted line in Fig. 8. At the downstream scour-
347 side, Fig. 8 shows that the data could be described by two main curves: i) an upper curve describing
348 the scour-profiles obtained with plunging (free-falling) jets, such as the case of the present study
349 without or with less effect of λ, the study of Ben Meftah and Mossa (2006) and that of Ghodsian et
350 al. (2012), where the different data tend to collapse onto each other; and ii) a lower characteristic
351 curve obtained as a result of the collapse of the scour-profiles caused by horizontal entering-jets,
352 such as in the studies by Balachandar and Kells (1997), Adduce and Sciortino (2006) and Espa and
353 Sibilia (2014). The data ranged between both curves, such as the case of runs R24 to R25 of the
354 present study, represent the scour-profiles obtained with a GCS of downstream sloped face with
355 significant λ-effect (see sec. 4.2). Fig.8 points out that the downstream scour-side is more
356 influenced by the entering-jet-flow typology than the upstream side.

357 The benefit of rescaling the scour profiles with this new approach leads to find a series of
358 typical profiles, describing the upstream and downstream sides of the scour hole under different
359 entering-jet-flow typologies. Each typical profile is generally predictable by the following closed-
360 form expression:

361
$$\begin{cases} \dfrac{z}{z_s} = -\left[2\left(\dfrac{X}{x_s}\right) - \left(\dfrac{X}{x_s}\right)^2 \right]^m & X \le x_s \\ \dfrac{z}{z_s} = -\left[2\left(1 + \dfrac{X - x_s}{l_s - x_s}\right) - \left(1 + \dfrac{X - x_s}{l_s - x_s}\right)^2 \right]^n & X \ge x_s \end{cases} \quad (8)$$

where m and n are constants to be found experimentally.

As previously mentioned, the scour profile is of asymmetric sides and the downstream side is more influenced by the entering-jet typology. In addition, the upstream side can also be affected by the GCS-dowstream slope. According to the experimental results shown in Fig. 8, for practitioners, the scour profile is predictable using Eq.(8) as follows: i) for the upstream scour-side ($X/x_s \leq 1$), in the case of a GCS of downstream vertical face or sloped face without λ-effect, Eq. (8) should be used with an exponent coefficient $m \approx 0.8$ (with an average error ranging from less than 2% to 35%), as shown in Fig. 8 by the bold solid curve, independent of the entering-jet typology and the GCS-features. When λ has significant effect, the downstream face of the GCS is completely exposed to the flow (all sediments on the GCS-face will be eroded), forming the upstream scour profile which is simply predictable as $z/z_s = -X/x_s$, as shown in Fig. 8 by the dotted line; and ii) for the downstream scour-side ($X/x_s \geq 1$), with plunging (free-falling) jet-flows, Eq. (8) should be used with an exponent coefficient $n \approx 3$ (with an average error ranging from less than 2% to 30%), as shown in Fig.8 by the bold solid curve. With horizontal jets, Eq. (8) should be used, however, with $n \approx 1.4$ (with an average error ranging from less than 2% to 27%), as shown in Fig.8 by the dashed curve. For a GCS of downstream sloped face with λ-effect, the profile of the downstream scour-side can be predicted by Eq. (8) averaging the values of the exponent coefficient n obtained with the plunging and horizontal jet typologies, i.e., $n \approx 2.2$. Table 2 shows a guidance for practitioners on how to use Eq. (8) and its limitations. To make Eq. (8) operational, the prediction of the three scour characteristic-lengths l_s, x_s, and z_s is fundamental. This will be the subject of the next section.

Prediction of the characteristic lengths of the equilibrium-scour hole

Prediction of scour dimensions downstream of hydraulic structures is challenging due to the complexity of phenomenon and its dynamic sensitivity to structure and sediment typologies. The majority of previous studies in this field have focused on deriving theoretical and empirical

equations to predict the dimensions of the equilibrium-scour hole. Most of these equations are not easily practicable because they require measurements of specific variables (field velocities, turbulent structures, jet diffusion coefficient, angle of repose of bed sediment, friction coefficients, etc.) and in some instances are not dimensionally homogeneous, as shown above in Eqs. (4-6). In this study, we propose new dimensionless equations to predict the characteristic lengths of the equilibrium-scour hole.

Based on the dimensional analysis of the processes, as shown in Eq. (3), in Fig. 9, we plot the normalized maximum scour depth at equilibrium z_s/h_s as a function of the dimensionless parameter Φ, where $\Phi = (1+z_d/h_s)^{a'}(h_t/h_s)^{b'}(\lambda/\pi)^{c'}(Fr_{sd})^{d'}$ and a', b', c', d' are constants to be found experimentally. It is worth mentioning that λ in the function Φ is in radians and $0° < \lambda \leq 90°$. In addition to the data of this study, in Fig. 9, we also plot previous results obtained by Bormann and Julien (1991), in a sand-bed channel of d_{50} ranging between 0.3 and 0.45 mm. The maximum eroded depth is normalized and presented as a function of a series of well-known variables, i.e., d_{50}, g, q, z_d, Δ, λ, and other variables that may be measured or computed using the initial flow conditions, i.e., h_s, h_t. As you can see, these variables are easy to define, which makes it adequate to predict the equilibrium-scour depth. Interpolating the data reported in Fig. 9, we obtain the following expression of the maximum scour depth at equilibrium:

$$\frac{z_s}{h_s} = 0.24\left(1+\frac{z_d}{h_s}\right)^{0.92}\left(\frac{h_t}{h_s}\right)^{0.24}\left(\frac{\lambda}{\pi}\right)^{-0.34}\left(Fr_{sd}\right)^{0.38} \quad (9)$$

Note that Eq. (9) is valid for a GCS, of rectangular crest, in bed rivers of medium to very coarse sand sediments. The 50%-deviation lines (lower and upper levels) from the best fit line of Eq. (9) are also illustrated in Fig. 9. Considering the complexity of the phenomenon, the uncertainty of predicting z_s using Eq. (9) is quite acceptable as compared to the uncertainty of other equations in the literature (Heng et al., 2013).

Fig. 10 shows the normalized downstream distance to the position of maximum eroded depth x_s/h_s as a function of the dimensionless parameter Φ', where Φ' is the same function as Φ but with different values of a', b', c', d'. In addition to the present study, other data collected by Bormann and Julien (1991) are also listed in Fig. 10. Fig. 10 indicates an overall increasing trend of x_s/h_s with the increase of Φ'. A linear regression analysis of these data leads to an expression for predicting x_s as follows:

$$\frac{x_s}{h_s} = 0.22\left(1+\frac{z_d}{h_s}\right)^{0.76}\left(\frac{h_t}{h_s}\right)^{0.68}\left(\frac{\lambda}{\pi}\right)^{-0.16}\left(Fr_{sd}\right)^{0.82} \tag{10}$$

The uncertainty of predicting x_s using Eq. (10) is indicated in Fig. 10 by the 50%-deviation lines from the best fit line. Eq. (10) covers the same range of validity as Eq. (9).

Fig. 11 depicts the dimensionless length of the equilibrium-scour hole l_s/z_s versus the dimensionless downstream distance to the position of maximum eroded depth x_s/z_s. Together with the data of the present study, in Fig. 11, previous data collected by Lenzi et al. (2003), Adduce and Sciortino (2006) and Ghodsian et al. (2012) are also plotted. Fig.11 highlights that the data of the various studies show a similar trend, leading to the following expression:

$$\frac{l_s}{z_s} = 2.16\frac{x_s}{z_s} \tag{11}$$

In Fig. 11, we also plot the 30%-deviation lines from the best fit line of Eq. (11) to indicate the uncertainty of l_s-prediction. It is important to point out that the scour holes in Lenzi et al. (2003), have been measured in six mountain rivers of natural mixed sediments, ranging from cobbles and boulders to gravel and sand particles. This indicates the large range of validity of Eq. (11) to various sediment properties.

Finally, using Eq. (8) with the help of Eqs. (9-11) one can obtain a reasonable prediction of the equilibrium-scour profile downstream of a GCS in sand-bed rivers. Given the type (design) of

the GCS and the initial hydraulic conditions, the extents and the eroded volume of the scour hole can be adequately predicted in advance.

Conclusions

The river erosion is a very complex process, playing a fundamental role in defining the morphology of waterways. Prediction of the sediment-transport dynamics is challenging due to the complex dependence on several factors, including sediment structures, waterway morphology, and flow properties. The highly intense rainfall due to extreme weather events, which are becoming more frequent, significantly increases runoff volumes that affect the river's stability. To deal with this problem, grade-control structures are often used in alluvial channels to limit bed degradation and maintain stream stability. Design of an effective grade-control structure must therefore include adequate protective measures against local downstream scour.

In the present study, we focus on the scour hole development downstream of a sloped grade-control structure in alluvial channels with uniform, non-cohesive sediment beds. Based on a series of laboratory experiments and referencing data collected from previous studies, new expressions are proposed to predict the temporal and equilibrium scour features that are representative of sand-bed rivers.

The experimental results show that the scour evolution is influenced by the slope, λ, of the downstream GCS-face. The reduction of λ is accompanied by an increase in the equilibrium-scour dimensions (depth and length) downstream of the GCS. In agreement with what observed in previous studies, the results show that the λ-effect should only occur with λ smaller than the slope of the upstream side of the scour hole obtained with a vertical face.

The results show that the scour process evolves in three distinct phases: a very rapid initial phase, an intermediate gradual phase, and a final equilibrium state. The intermediate phase shows a considerable data-scattering between the different scour analyzed conditions. This indicates that the

scour evolution during the intermediate phase seems more influenced by the GCS geometry and the hydraulic condition. In the present study, a general empirical expression to predict the scour hole evolution with time is proposed and well-defined for the different analyzed GCSs. This expression is valid for sand-bed rivers of uniform granulometry, but it can adapt to many other conditions, i.e., gravel-bed rivers, bed with mixed sediments, GCSs of different geometries.

With the scope to achieve complete similarity between the equilibrium-scour profiles, in the present study, a new scaling approach is proposed. This new scaling approach significantly improves the similarity of the scour profiles, restricting them to go through three well-defined coordinates. The scaling of the scour profiles with this new approach indicates a slight asymmetry between the upstream and downstream scour-sides. Based on the present and previous experimental data, new equations for predicting the equilibrium-scour profile at both sides are proposed. These equations are classified into different categories following the nature of the entrance jet-flow. A guidance for practitioners on how to use these equations and their limitations is provided. Although the findings are limited to the present study, the new scaling approach is suitable for any scour downstream a hydraulic structure (of any geometry) in any bed-river condition (of cohesive or non-cohesive, uniform or mixed, fine or coarse sediments, etc.). Therefore, the general equation predicting the equilibrium-scour profile, obtained as a result of this scaling approach, could be further adaptable to many other scouring problems, defining only the suitable values of its power coefficients m and n. To achieve this goal, further studies on other scouring conditions are recommended.

In order to make the proposed scour-profile equations soluble, in this study, we also developed a series of new equations to predict l_s, x_s, and z_s of the equilibrium scour hole. These equations are expressed as a function of variables that are easy to define by practitioners. The use of the general equation predicting the equilibrium-scour profile with the help of l_s-, x_s-, and z_s-equations facilitates the prediction of the equilibrium-scour profile downstream of a GCS. This proposed approach for

predicting equilibrium-scour profile downstream of a GCS is very simple to apply for sand-bed rivers and can be adapted to many other scouring problems with different structures and various sediment properties.

Acknowledgement

The experiments were carried out at the Hydraulic Laboratory of the Mediterranean Agronomic Institute of Bari (Italy).

Notations

B	Channel width (m)
b_s	Width of the GCS (m)
d_{50}	Sediment median size (m)
d_{90}	Grain size for which 90% of sampled particles are finer (m)
Fr_s	Froude number at the crest-end of flow depth h_s (-)
Fr_{sd}	Sediment densimetric Froude number (-)
g	Gravity acceleration ($m.s^{-2}$)
H	Head drop (m)
hs	Entering-jet thickness (m)
h_t	Tailwater depth above unscoured bed level (m)
L_s	Entering-jet diffused length (m)
l_s	Equilibrium-scour length (m)
Q	Water discharge ($m^3.s^{-1}$)
Re	Reynolds number (-)
q	Unit water discharge ($m^2.s^{-1}$)
t	Time (s)
t_e	Time required to achieve the equilibrium stage (s)
U_0	Entering-jet velocity ($m.s^{-1}$)
x, y, z	Longitudinal, lateral and vertical coordinates, respectively (m)
X	(x-x') Horizontal distance from the GCS-face (m)
x_s	x-Position from the GCS-face at which the scour attains its maximum depth (m)
x'	Base length of the downstream GCS-face at the original-bed level (m)
z_d	Drop height of the GCS (m)
z_m	Temporal maximum scour depth (m)
z_s	Maximum equilibrium-scour depth (m)
α	Equilibrium side angle of scour hole (radians)
β	Entering-jet angle near bed (radians)
Δ	Sediment to water density ratio (-)
Φ, Φ'	Dimensionless parameter (-)
λ	Downstream-face angle of the GCS (radians)
ν	Kinematic water viscosity ($m^2.s^{-1}$)
ρ_s	Sediment density ($kg.m^{-3}$)

ρ_w Water density (kg.m^{-3})

References

Adduce, C., Sciortino, G. (2006). "Scour due to a horizontal turbulent jet: Numerical and experimental investigation." *Journal of Hydraulic Research* 44(9), 663-673. https://doi.org/10.1080/00221686.2006.9521715

Balachandar, R., Kells, J.A. (1997). "Local channel in scour in uniformly graded sediments: the time-scale problem." *Canadian Journal of Civil Engineering* 24(10), 799-807. https://doi.org/10.1139/l97-034

Ben Meftah, M., Mossa, M. (2006). "Scour holes downstream of bed sills in low-gradient channels." *Journal of Hydraulic Research* 44(7), 497-509. https://doi.org/10.1080/00221686.2006.9521701

Bormann, N.E, Julien, P.Y., (1991). "Scour downstream of grade-control structures." *Journal of Hydraulic Engineering* 117(5), 579-594. https://doi.org/10.1061/(ASCE)0733-9429(1991)117:5(579)

Carstens, M.R. (1966). "Similarity laws for localized scour." *Journal of the Hydraulics Division* 92(3), 13-34.

Chen, J., Hsu, H., Hong, Y. (2016). "The influence of upstream slope on the local scour at drop structure." *Journal of Mountain Science* 13(12), 2237-2248. https://doi.org/10.1007/s11629-015-3790-5

D'Agostino, V., Ferro, V. (2004). "Scour on alluvial bed downstream of grade-control structures." *Journal of Hydraulic Engineering* 130(1), 24-37. https://doi.org/10.1061/(ASCE)0733-9429(2004)130:1(24)

Espa, P., Sibilla, S. (2014). "Experimental study of the scour regimes downstream of an apron for intermediate tailwater depths." *Journal of Applied Fluid Mechanics* 7(4), 611-624. https://doi.org/ 10.1201/9781439833865.ch185

Fakhari, Z., Kabiri-Samani, A. (2017). "Scour in the transition from super- to subcritical flow without a hydraulic jump." *Journal of Hydraulic Research* 55(4), 470-479. https://doi.org/10.1080/00221686.2016.1275052

Farhoudi, J., Shayan, H.K. (2014). "Investigation on local scour downstream of adverse stilling basins." *Ain Shams Engineering Journal* 5(6), 361-375. https://doi.org/10.1016/j.asej.2014.01.002

Gaudio, R., Marion, A., Bovolin, V. (2000). "Morphological effects of bed sills in degrading rivers." *Journal of Hydraulic Research* 38(3), 89-96. https://doi.org/10.1080/00221680009498344

Ghodsian, M., Mehraein, M., Ranjbar, H.R. (2012). "Local scour due to free fall jets in non-uniform sediment." *Scientia Iranica* 19(12), 1437-1444. https://doi.org/10.1016/j.scient.2012.10.008

Guan, D., Melville, B., Friedrich, H. (2016). "Local scour at submerged weirs in sand-bed channels." *Journal of Hydraulic Research* 54(3), 172-184. https://doi.org/10.1080/00221686.2015.1132275

518 Guan, D., Melville, B.W., Friedrich, H. (2014). "Flow patterns and turbulence structures in a scour hole downstream of
519 a submerged weir." *Journal of Hydraulic Engineering* 140(1), 68-76. https://doi.org/10.1061/(ASCE)HY.1943-
520 7900.0000803
521 Guven, A., Gunal, M. (2008). "Prediction of scour sownstream of grade-control structures using neural networks."
522 *Journal of Hydraulic Engineering* 134(11), 1656-1660. https://doi.org/10.1061/(ASCE)0733-
523 9429(2008)134:11(1656)
524 Heng, S., Tingsanchali, T., Suetsugi, T. (2013). "Prediction formulas of maximum scour depth and impact location of a
525 local scour hole below a chute spillway with a flip bucket." *WIT Transactions on Ecology and the Environment*
526 172, 251-262. https://doi.org/10.2495/RBM130211
527 Hill, D.F., Younkin, B.D. (2006). "PIV measurements of flow in and around scour holes. *Experiments in Fluids* 41(8),
528 295-307. https://doi.org/10.1007/s00348-006-0156-3
529 Hopfinger, E.J., Kurniawan, A., Graf, W.H., Lemmin, U. (2004). "Sediment erosion by Görtler vortices: the scour-hole
530 problem." *Journal of Fluid Mechanics* 520(12), 327-342. https://doi.org/10.1017/S0022112004001636
531 Kuhnle, R.A., Alonso, C.V., Shields, F.D. (2002)."Local scour associated with angled spur dikes." *Journal of Hydraulic*
532 *Engineering* 128(12), 1087-1093. https://doi.org/10.1061/(ASCE)0733-9429(2002)128:12(1087)
533 Laursen, E.M. (1952). "Observations on the nature of scour." *Proc*, *5th Hydr. Conf.*, *Bull*. 34, Univ. of Iowa, Iowa City,
534 Iowa, 179-197.
535 Lenzi, M.A., Marion, A., Comiti, F. (2003). "Local scouring at grade-control structures in alluvial mountain rivers"
536 *Water Resources Research* 39(7), 1176. https://doi.org/10.1029/2002WR001815
537 Lu, J.Y., Hong, J.H., Chang, K.P., Lu, T.F. (2013). "Evolution of scouring process downstream of grade-control
538 structures under steady and unsteady flows." *Hydrological Processes* 27 (9), 2699-2709.
539 https://doi.org/10.1002/hyp.9318
540 Martins, R. (1975). "Scouring of rocky river beds and free-jet spillways." *Int. Water Power Dam Constr.* 27(5), 152-
541 153.
542 Mason, P.J., Arumugam, K. (1985). "Free jet scour below dams and flip buckets." *Journal of Hydraulic Engineering*
543 111(2), 220-235. https://doi.org/10.1061/(ASCE)0733-9429(1985)111:2(220)
544 Mossa, M. (1998). "Experimental study on the scour downstream of grade-control structures." conference: *XXVI*
545 *Convegno di Idraulica e Costruzioni Idrauliche*, Catania, Italy, 581-594.
546 Nasrollahi, A., Ghodsian, M., Neyshabouri, S.A.A.S. (2008). "Local scour at permeable spur dikes." *Journal of Applied*
547 *Sciences* 8(12), 3398-3406. https://doi.org/10.3923/jas.2008.3398.3406

548 Pagliara, S., Amidei, M., Hager, W.H. (2008a). “Hydraulics of 3D plunge pool scour.” *Journal of Hydraulic*
549 *Engineering* 134(9), 1275-1284. https://doi.org/10.1061/(ASCE)0733-9429(2008)134:9(1275)
550 Pagliara, S., Hager, W.H., Unger, J. (2008b). “Temporal evolution of plunge pool scour.” *Journal of Hydraulic*
551 *Engineering* 134(11), 1630-1638. https://doi.org/10.1061/(ASCE)0733-9429(2008)134:11(1630)
552 Pagliara, S., Palermo, M., Carnacina, I. (2011) “Expanding pools morphology in live-bed conditions.” *Acta Geophysica*
553 59(2), 296-316. https://doi.org/10.2478/s11600-010-0048-z
554 Pagliara, S., Palermo, M. (2013) “Rock grade control structures and stepped gabion weirs: Scour analysis and flow
555 features.” *Acta Geophysica* 61(1), 126-150. https://doi.org/10.2478/s11600-012-0066-0
556 Papanicolaou, A.N., Bressan, F., Fox, J., Kramer, C., Kjos, L. (2018). “Role of structure submergence on scour
557 evolution in gravel bed rivers: application to slope-crested structures.” *Journal of Hydraulic Engineering*
558 144(2), 1087-1093. https://doi.org/10.1061/(ASCE)HY.1943-7900.0001411
559 Schoklitsch, A. (1932). “Kolkbidung unter uberfallstrahlen.” *Die Wasserwirtschaft*.
560 Scurlock, S.M., Thornton, C.I., Abt, S.R. (2012). “Equilibrium scour downstream of three-dimensional grade-control
561 structures.” *Journal of Hydraulic Engineering* 138(2), 167-176. https://doi.org/10.1061/(ASCE)HY.1943-
562 7900.0000493
563 Shafai-Bejestan, M., Nabavi, S.M.R., Dey, S. (2016). “Scour downstream of grade control structures under the
564 influence of upward seepage.” *Acta Geophysica* 64(6), 694-710. https://doi.org/10.1515/acgeo-2016-0024
565 Tregnaghi, M., Marion, A., Gaudio, R. (2007). “Affinity and similarity of local scour holes at bed sills.” *Water*
566 *Resources Research* 43(11), W11417. https://doi.org/10.1029/2006WR005559
567 Veronese, A. (1937). “Erosioni di fondo a valle di uno scarico.” *Ann. Lav. Pubblici* 75(9), 717-726.
568 Wang, L., Melville, B.W., Guan, D., Whittaker, C.N. (2018). “Local scour at downstream sloped submerged weirs.”
569 *Journal of Hydraulic Engineering* 144(8), 04018044. https://doi.org/10.1061/(ASCE)HY.1943-7900.0001492
570 Yang, S.Q., Tan, S.K., Wang, X.K. (2012). “Mechanism of secondary currents in open channel flows.” Journal of
571 Geophysical Research: Earth Surface 117(F4), F04014(1-13). https://doi.org/10.1029/2012JF002510
572
573
574
575
576

577

578 **Table 1.** Experimental hydraulic conditions of this study..

Runs	q (m^2/s)	λ (°)	h_t (m)	x_s (m)	l_s (m)	z_s (m)	h_s (m)	Fr_{sd} (-)
R1	0.003	90	0.029	0.06	0.14	0.04	0.007	2.72
R2	0.007	90	0.030	0.10	0.24	0.07	0.010	3.83
R3	0.010	90	0.029	0.13	0.33	0.11	0.014	4.06
R4	0.007	90	0.052	0.10	NI	0.06	0.020	1.87
R5	0.008	90	0.067	0.10	NI	0.04	0.012	3.94
R6	0.008	90	0.075	0.10	NI	0.03	0.011	3.91
R7	0.008	90	0.062	0.11	NI	0.04	0.011	3.87
R8	0.012	90	0.037	0.18	0.48	0.14	0.015	4.38
R9	0.013	90	0.064	0.12	0.29	0.09	0.016	4.45
R10	0.012	90	0.071	0.14	NI	0.10	0.003	4.32
R11	0.013	90	0.077	0.12	NI	0.08	0.016	4.43
R12	0.020	90	0.085	0.12	NI	0.06	0.023	4.78
R13	0.003	45	0.023	0.05	0.13	0.05	0.007	2.81
R14	0.007	45	0.030	0.10	0.29	0.09	0.011	3.83
R15	0.009	45	0.065	0.10	NI	0.08	0.012	3.95
R16	0.009	45	0.080	0.07	0.17	0.06	0.011	4.68
R17	0.010	45	0.057	0.11	NI	0.10	0.014	3.89
R18	0.011	45	0.073	0.11	NI	0.09	0.014	4.18
R19	0.011	45	0.034	0.14	0.41	0.13	0.014	4.39
R20	0.013	45	0.072	0.14	0.36	0.11	0.016	4.74
R21	0.015	45	0.085	0.12	NI	0.10	0.017	4.89

R22	0.015	45	0.067	0.14	NI	0.13	0.017	4.91
R23	0.015	45	0.077	0.13	NI	0.11	0.017	4.91
R24	0.005	18	0.025	0.116	0.18	0.04	0.010	2.65
R25	0.009	18	0.030	0.272	0.43	0.09	0.014	3.37
R26	0.013	18	0.035	0.4175	0.67	0.14	0.018	3.97
R27	0.014	18	0.086	0.19	NI	0.06	0.020	3.81
R28	0.014	18	0.079	0.205	NI	0.09	0.019	4.20
R29	0.010	18	0.081	0.16	NI	0.05	0.016	3.48
R30	0.011	18	0.034	0.29	NI	0.11	0.016	3.71
R31	0.012	18	0.061	0.205	NI	0.08	0.018	3.72
R32	0.014	18	0.062	0.321	NI	0.04	0.020	4.07

NI: not identified

Table 2. New proposed expressions to predict the scour profile at equilibrium. It should be noted herein that these formulas were obtained with GCSs, of horizontal rectangular crest, in sand-bed channels with clear-water condition and of Fr_{sd} ranging from 1 to 70.

Position	Application conditions	Formula
$X/x_s \leq 1$ (upstream side of the scour profile)	GCS of downstream vertical-face or sloped-face without λ-effect	$\frac{z}{z_s} = -\left[2\left(\frac{X}{x_s}\right) - \left(\frac{X}{x_s}\right)^2\right]^{0.8}$ A variation of the power coefficient 0.8 by ±35% gives the upper (+) and lower (-) maximum deviations from the best fit line obtained with 0.8.
	GCS of downstream sloped-face with λ-effect: Face completely exposed to flow	$\frac{z}{z_s} = -\frac{X}{x_s}$ Profile of the downstream GCS-face
$X/x_s \geq 1$ (downstream side of the scour profile)	GCS of downstream vertical-face or sloped-face without λ-effect: Plunging /free-fall jet	$\frac{z}{z_s} = -\left[2\left(1+\frac{X-x_s}{l_s-x_s}\right) - \left(1+\frac{X-x_s}{l_s-x_s}\right)^2\right]^{3}$ The upper (+)/lower (-) maximum deviation from the best fit line is obtainable by varying the power coefficient 3 by ±30%.
	GCS of downstream sloped-face with λ-effect	$\frac{z}{z_s} = -\left[2\left(1+\frac{X-x_s}{l_s-x_s}\right) - \left(1+\frac{X-x_s}{l_s-x_s}\right)^2\right]^{2.2}$ The upper (+)/lower (-) maximum deviation from the best fit line is obtainable by varying the power coefficient 2.2 by ±22%.
	GCS followed by horizontal long rigid apron of same height as the original bed profile: Horizontal jet	$\frac{z}{z_s} = -\left[2\left(1+\frac{X-x_s}{l_s-x_s}\right) - \left(1+\frac{X-x_s}{l_s-x_s}\right)^2\right]^{1.4}$ The upper (+)/lower (-) maximum deviation from the best fit line is obtainable by varying the power coefficient 1.4 by ±28%.

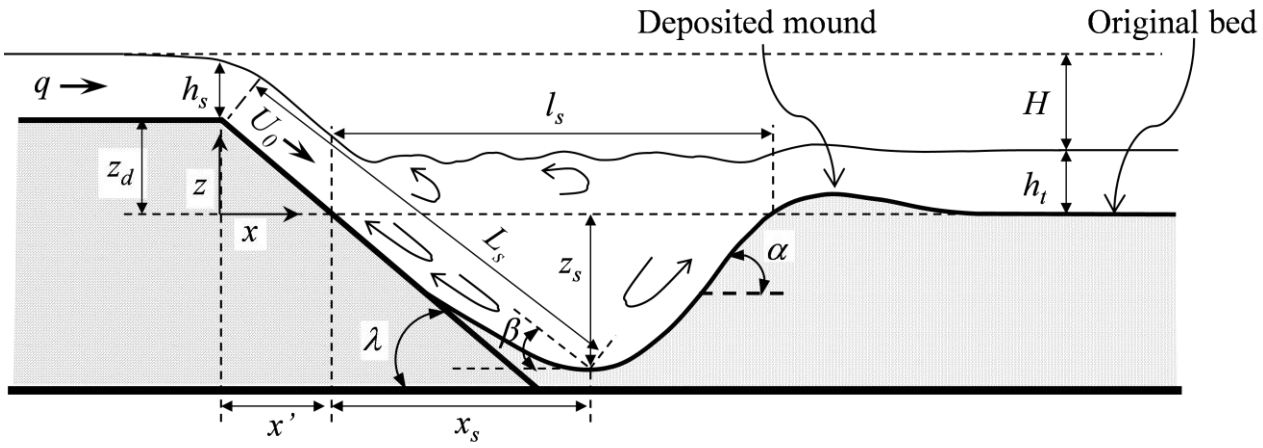

600

601 **Fig. 1.** Definition sketch of the scour hole downstream of the GCS. Note that *x*' depends upon the slope of the

602 downstream GCS-face, *x*' = 0 with the vertical face.

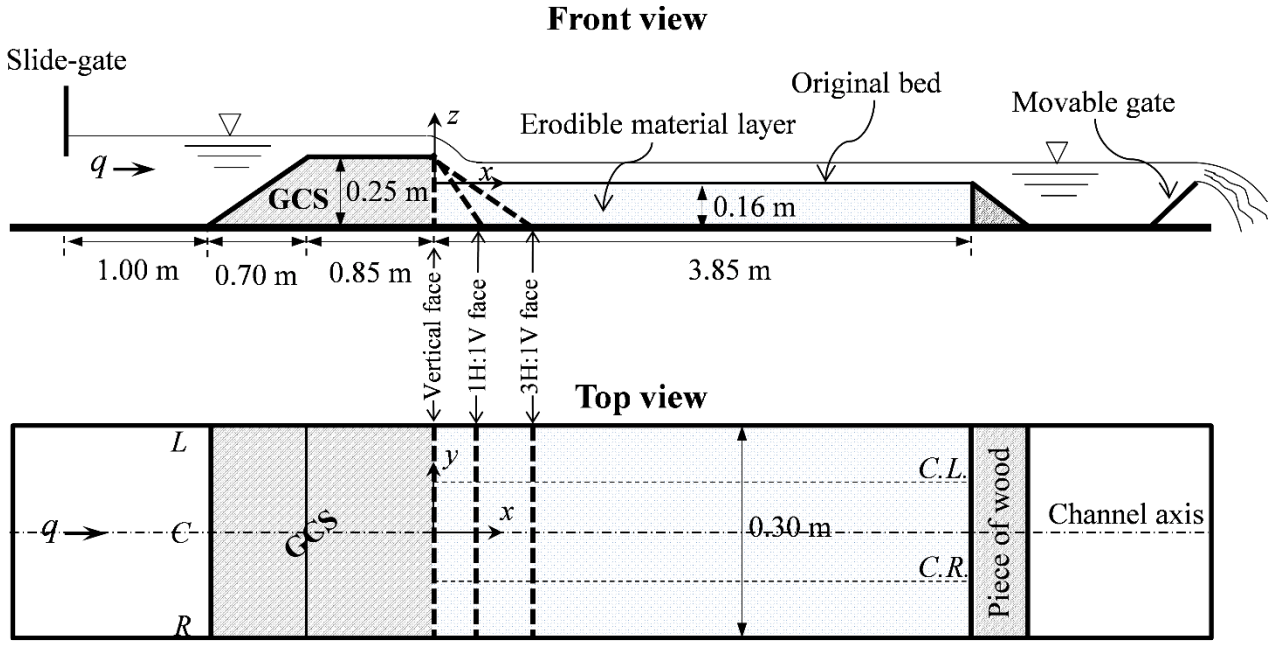

603

604 **Fig. 2.** Schematic view of the experimental setup. The three downstream GCS-faces are represented by the bold dashed

605 lines. L indicates the left wall-side of the channel, R is the right wall side, C is the centerline (channel axis), C.L. is the

606 centerline of the left half part of the channel and C.R is the centerline of the right half part.

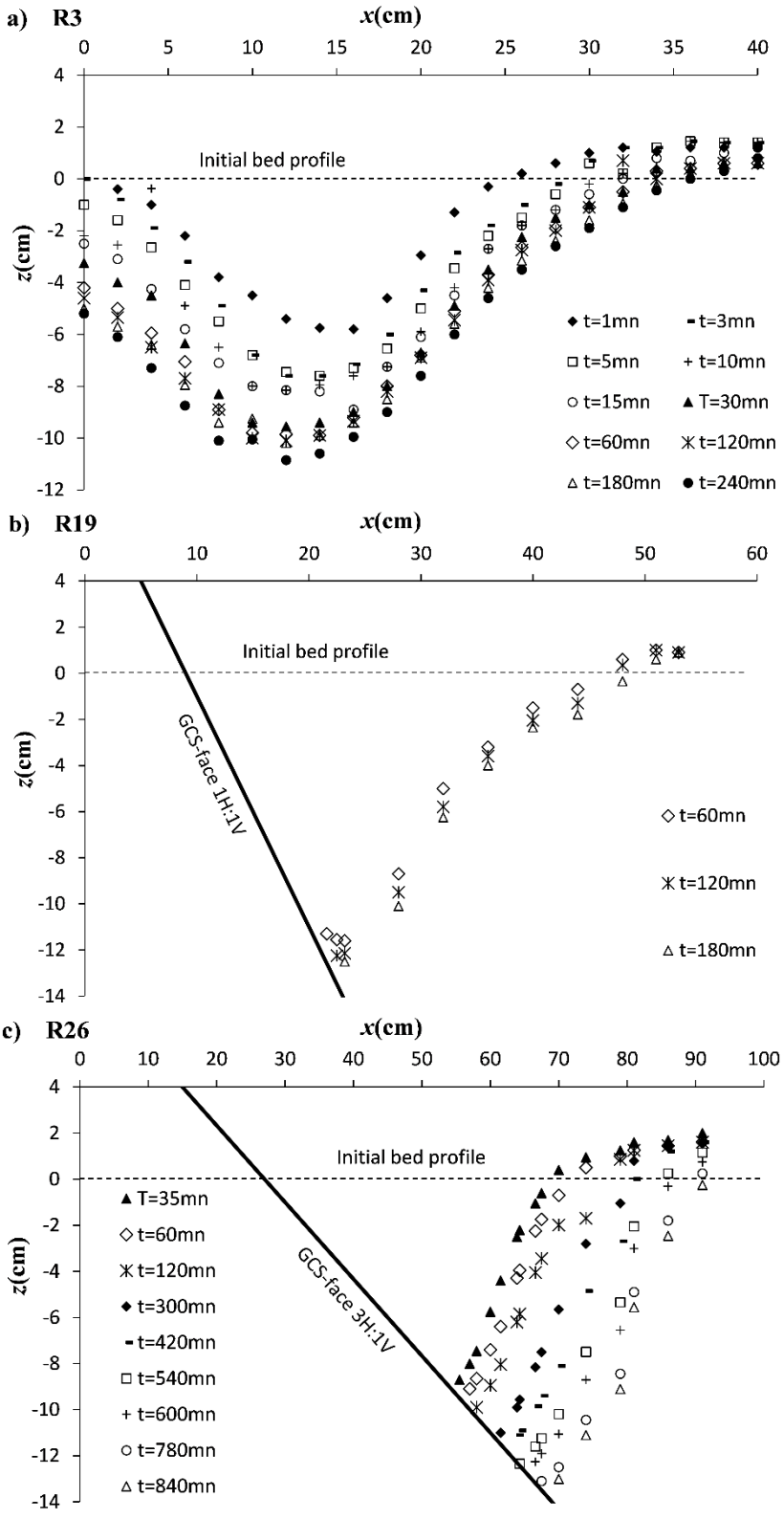

Fig. 3. Scour hole evolution as a function of time: a) run R3, vertical face (λ=90°), q = 0.010 m^2/s, h_t = 0.029 m; b) run R19, 1H:1V face (λ = 45°), q = 0.011 m^2/s, h_t = 0.034 m; c) run R26, 3H:1V face (λ = 18°), q = 0.013 m^2/s, h_t = 0.035 m.

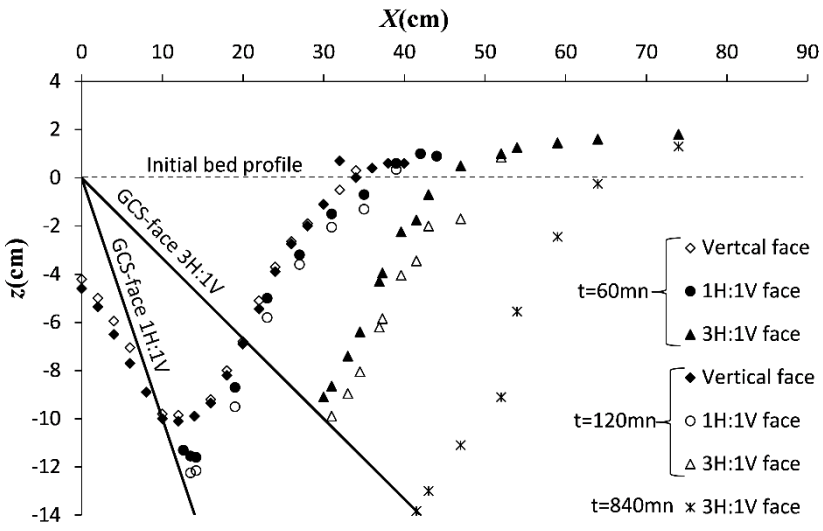

613

614 **Fig. 4.** λ-Effect on the scour features. Note that, with a sloped GCS-face (1H:1V or 3H:1V), a part or all the upstream

615 scour-side profile is represented by the downstream GCS-face.

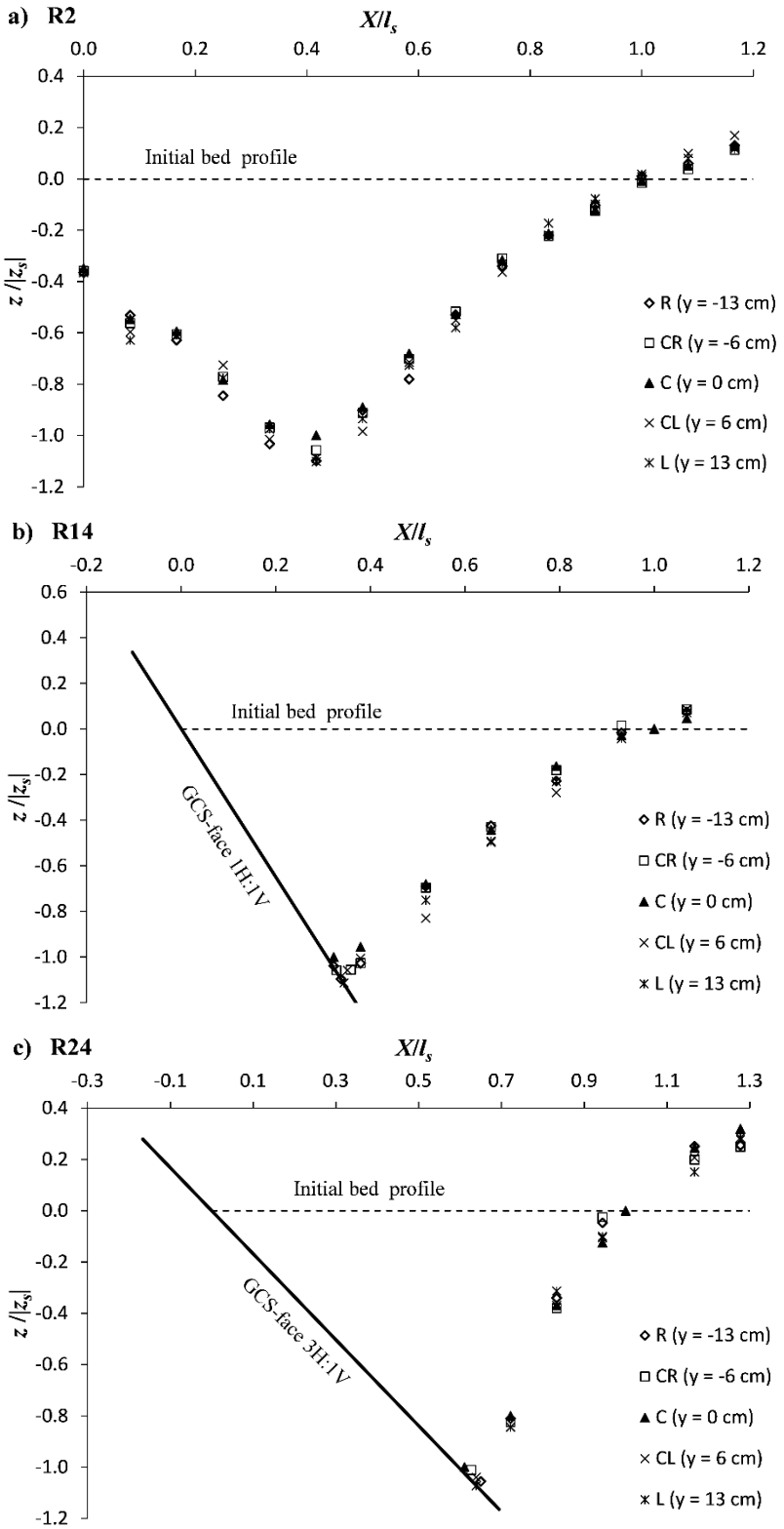

616

617

618

619

620 **Fig. 5.** Profiles of the equilibrium scour at different transversal positions: a) run R2, vertical face ($\lambda = 90°$), $q = 0.007$

621 m^2/s, $h_t = 0.030$ m; b) run R14, 1H:1V face ($\lambda = 45°$), $q = 0.007$ m^2/s, $h_t = 0.030$ m; c) run R24, 3H:1V face ($\lambda = 18°$), q

622 $= 0.005$ m^2/s, $h_t = 0.025$ m. $y = 0$ at the channel centerline C.

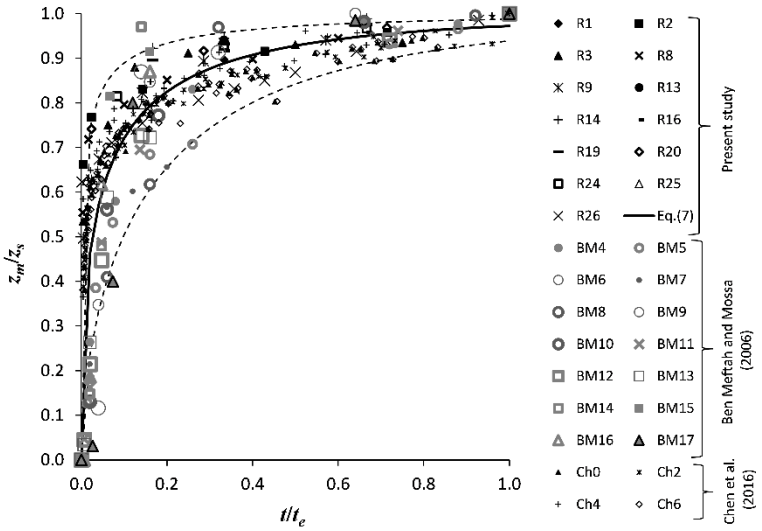

623

624 **Fig. 6.** Time evolution of the scour depth. The bold solid line is the solution of Eq. (7) with $a = 3.6$ and $b = 0.45$. The

625 dashed lines indicate the lower and upper maximum deviation from the best fit line (bold solid line): the upper deviation

626 line is obtainable by increasing the coefficient a by 22% from 3.6 and decreasing the coefficient b by 34% from 0.45,

627 and the lower deviation obtainable by decreasing a by 22% from 3.6 and increasing b by 34% from 0.45.

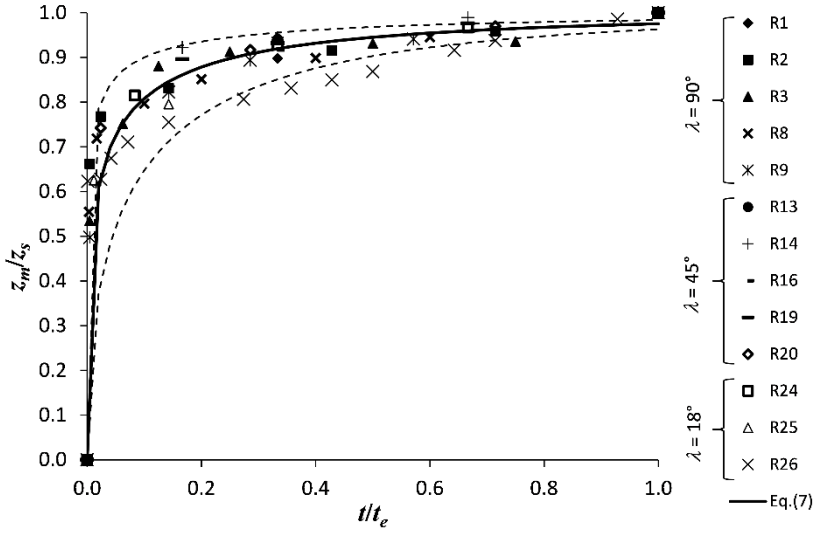

628

629 **Fig. 7.** Time evolution of the scour depth for the present study. The bold solid line is the solution of Eq. (7) with $a = 3.7$

630 and $b = 0.35$. The dashed lines indicate the lower (decreasing a by 11% from 3.7 and increasing b by 29% from 0.35)

631 and upper (increasing a by 11% from 3.7 and decreasing b by 29% from 0.35) maximum deviation from the best fit line

632 (bold solid line).

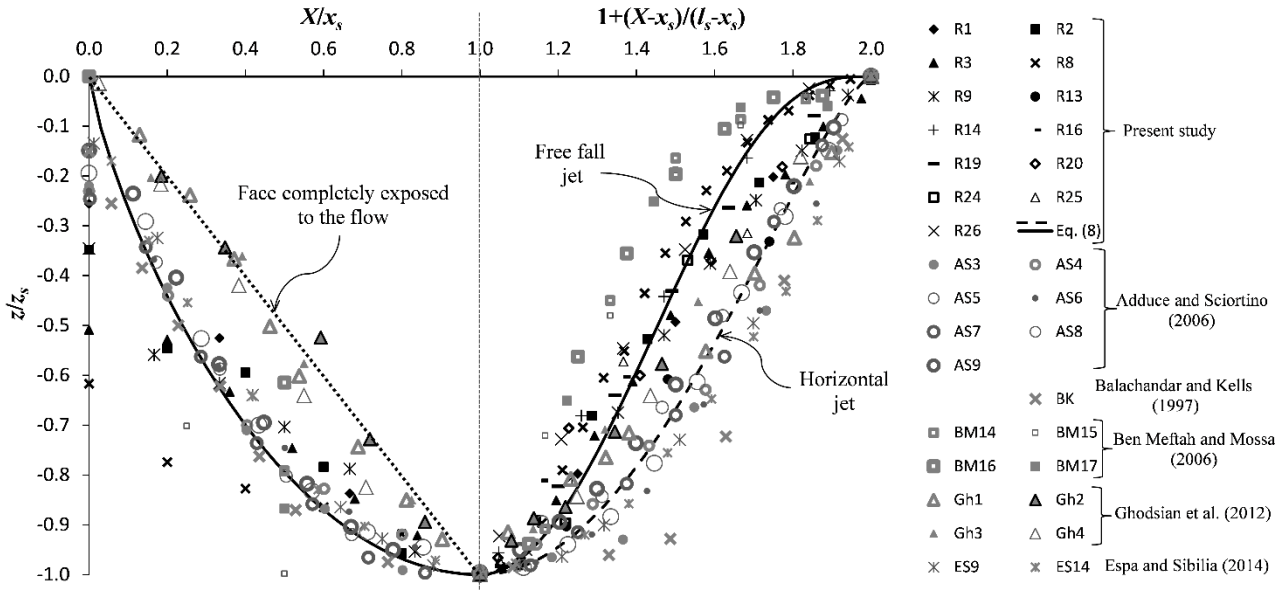

633

634 **Fig. 8.** Similarity of the scour hole profile at equilibrium. AS3 - AS9 measured data (horizontal jet) for Test 3 to 9 in
635 Adduce and Sciortino (2006), BK measured data (horizontal jet) in Balachandar and Kells (1997), BM14 - BM17
636 measured data (vertical bed sills) for Test 14 to 17 in Ben Meftah and Mossa (2006), Gh1 - Gh4 measured data (free fall
637 jet) with a geometric standard deviation of the bed material equal to, 1.3, 2.15, 2.31, 2.7, respectively, in Ghodsian et al.
638 (2012) and SE9-SE14 measured data (horizontal jet) for Test 9 and 14 in Espa and Sibilia (2014). The data were
639 obtained in medium to very coarse sand bed channels.

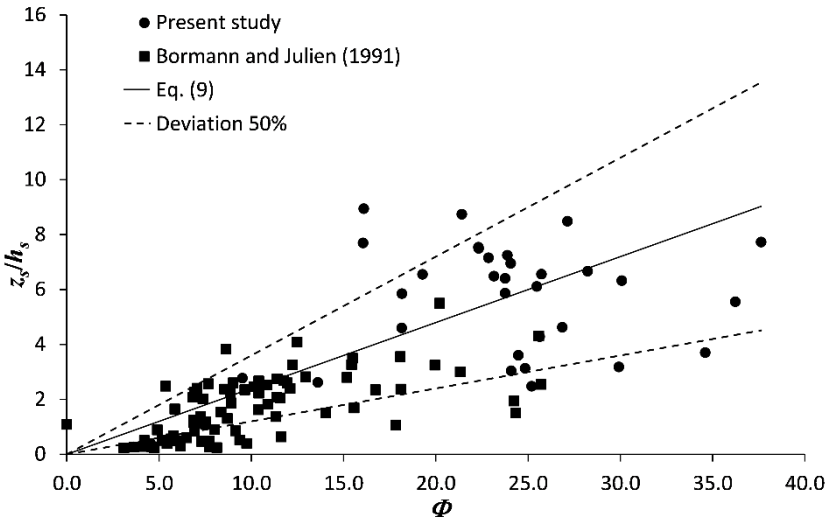

640

641 **Fig. 9.** Trend of the normalized equilibrium maximum-scour depth as a function of Φ. Herein, $\Phi = (1 +$
642 $z_d/h_s)^{a'}(h_t/h_s)^{b'}(\lambda/\pi)^{c'}(Fr_{sd})^{d'}$, λ in radians and $a' = 0.92$, $b' = 0.24$, $c' = -0.34$, $d' = 0.38$.

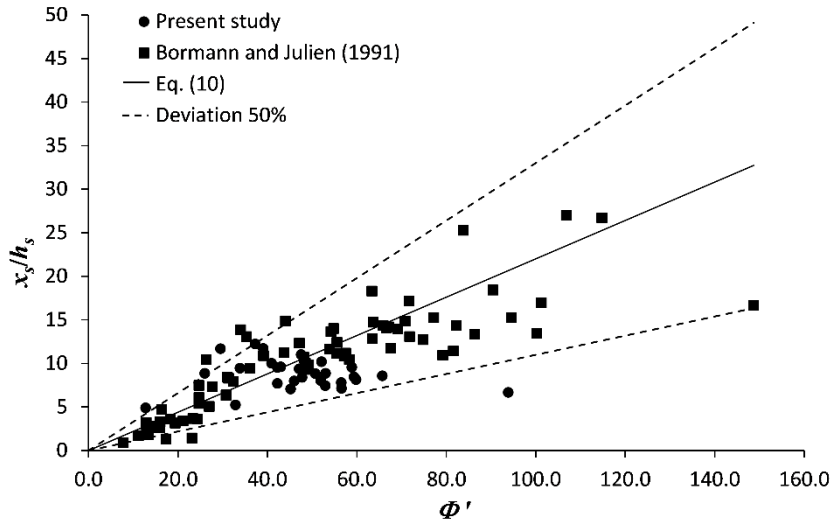

643

644 **Fig. 10.** Trend of the normalized downstream position of the maximum scour depth as a function of Φ'. Herein, $\Phi' = (1$

645 $+ z_d/h_s)^{a'}(h_t/h_s)^{b'}(\lambda/\pi)^{c'}(Fr_{sd})^{d}$, λ in radians and $a' = 0.76$, $b' = 0.68$, $c' = -0.16$, $d' = 0.82$.

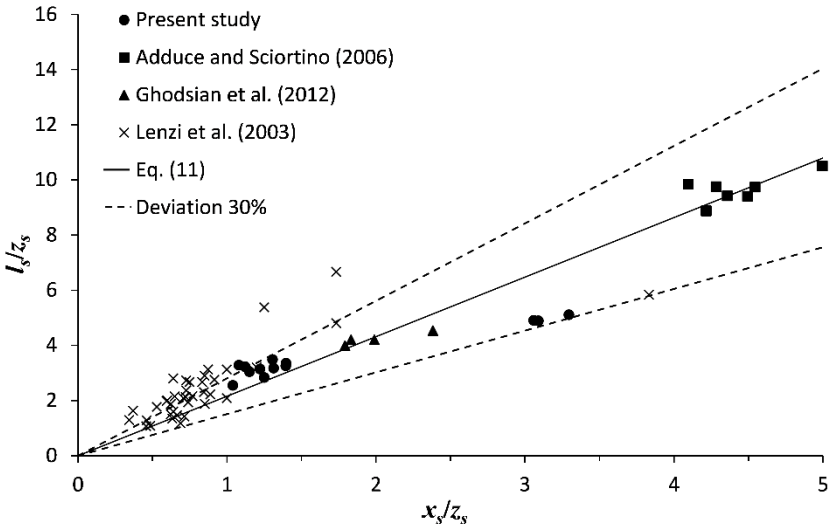

646

647 **Fig. 11.** Dimensionless length of the scour hole as a function of x_s/z_s.

648